

Experimental characterization of the electronic structure of anatase TiO₂: Thermopower modulation

Yuki Nagao¹, Akira Yoshikawa¹, Kunihiro Koumoto¹, Takeharu Kato², Yuichi Ikuhara^{2,3}, and Hiromichi Ohta^{1,4,a)}

¹*Graduate School of Engineering, Nagoya University, Furo-cho, Chikusa, Nagoya 464-8603, Japan*

²*Nanostructures Research Laboratory, Japan Fine Ceramics Center, 2-4-1 Mutsuno, Atsuta, Nagoya 456-8587, Japan*

³*Institute of Engineering Innovation, The University of Tokyo, 2-11-16 Yayoi, Bunkyo, Tokyo 113-8656, Japan*

⁴*PRESTO, Japan Science and Technology Agency, Sanbancho, Tokyo 102-0075, Japan*

Thermopower (S) for anatase TiO₂ epitaxial films (n_{3D} : 10^{17} – 10^{21} cm⁻³) and the gate voltage (V_g) dependence of S for thin film transistors (TFTs) based on TiO₂ films were investigated to clarify the electronic density of states (DOS) around the conduction band bottom. The slope of the $|S|$ - $\log n_{3D}$ plots was -20 μ VK⁻¹, which is an order magnitude smaller than that of semiconductors (-198 μ VK⁻¹), and the $|S|$ values for the TFTs increased with V_g in the low V_g region, suggesting that the extra tail states are hybridized with the original conduction band bottom.

Anatase TiO₂ has received increased attention for several optoelectronic applications, including photocatalysts¹ and dye-sensitized solar cells.² Because most of these types of optoelectronic functions in TiO₂ depend on the electronic density of states (DOS) around the bandgap between the O 2p valence band and the Ti 3d conduction band,³ numerous studies have examined the DOS around the bandgap.^{4–11} To experimentally clarify the DOS, X-ray and/or ultraviolet photoelectron spectroscopy is used for the valence band, while inverse photoelectron spectroscopy (IPES) is used for the conduction band.^{4–8} However, clarifying the DOS around the conduction band bottom is very difficult due to the insufficient energy resolution of IPES (~100 meV¹²). Therefore, an *ab initio* band calculation is mainly used to clarify the DOS around the conduction band bottom for anatase TiO₂.^{9–11}

In the present study, we aimed to clarify the DOS around the conduction band bottom by examining the thermopower (S) of anatase TiO₂ epitaxial films. The S value is an effective physical property because it reflects the energy differential of the DOS at the Fermi energy, $[\partial\text{DOS}(E)/\partial E]_{\text{EF}}$. Furthermore, the S value depends on the three-dimensional carrier concentration ($n_{3\text{D}}$). In particular, a field effect transistor structure is appropriate to measure the S values of semiconductors with different $n_{3\text{D}}$ because the gate voltage (V_{g}) can modulate $n_{3\text{D}}$ of a FET.^{13–15} Although many studies have reported powder,¹⁶ film growth^{17, 18} and FET fabrication^{19, 20} of anatase TiO₂, few have examined the S value of anatase TiO₂.^{21–23}

Herein we report the S values for anatase TiO₂ epitaxial films ($n_{3\text{D}}$: 10^{17} – 10^{21} cm⁻³) and the V_{g} dependence of S for a thin film transistor (TFT, on/off ratio $>10^4$, field effect mobility ~ 0.9 cm²V⁻¹s⁻¹) based on an undoped TiO₂ epitaxial film. We found that the slope of the $|S|$ - $\log n_{3\text{D}}$ plots for anatase TiO₂ films is ~ -20 μVK^{-1} , which is an order magnitude smaller than that of semiconductors with a parabolic DOS (-198 $\mu\text{VK}^{-1} = -\ln 10 \cdot k_{\text{B}}/e$), and $|S|$ values for TFTs increase with V_{g} in the low V_{g} region,

suggesting that the extra tail states are hybridized with the original conduction band bottom.

We fabricated several anatase TiO₂ epitaxial films by pulsed laser deposition (PLD, KrF excimer laser, 20 ns, $\sim 1 \text{ J cm}^{-2} \text{ pulse}^{-1}$, 10 Hz) on stepped (001) LaAlO₃ substrates at 700°C using Nb-doped or undoped rutile TiO₂ ceramic as targets. Reflection high energy electron diffraction, high resolution X-ray diffraction, and topographic AFM studies of the resultant films revealed that highly 001 oriented epitaxial TiO₂ (anatase) films were obtained with an epitaxial relationship (001)[100]TiO₂ || (001)[100] LaAlO₃. The TiO₂ film thicknesses, which were measured by grazing incidence X-ray reflection, were ~ 100 nm. Figure 1 shows a cross sectional high-resolution transmission electron microscope (HRTEM) image of a TiO₂ film grown on (001) LaAlO₃, confirming heteroepitaxial growth of TiO₂. An abrupt heterointerface was observed between the TiO₂ film and the LaAlO₃ substrate.

Then we measured the carrier concentration (n_{3D}) and Hall mobility (μ_{Hall}) of the TiO₂ films [Fig. 2(a)], which were fabricated using undoped or Nb-doped TiO₂ ceramic targets by the dc four probe method with a van der Pauw electrode configuration at room temperature (RT). μ_{Hall} was independent of n_{3D} ($\sim 7 \text{ cm}^2 \text{ V}^{-1} \text{ s}^{-1}$, which corresponds well to the literature value $\sim 10 \text{ cm}^2 \text{ V}^{-1} \text{ s}^{-1}$) in the lower n_{3D} region (undoped films, $n_{3D} < 10^{20} \text{ cm}^{-3}$). However, an n_{3D} dependence ($\sim n_{3D}^{-2/3}$) appeared in the higher n_{3D} region (Nb-doped films, $n_{3D} > 10^{20} \text{ cm}^{-3}$), indicating that ionized impurity scattering predominantly occurs in the higher n_{3D} region.

Figure 2b shows the $|S|$ - $\log n_{3D}$ plots for the TiO₂ films, which were measured using the conventional steady state method at RT. The negative S values indicated the films have an n -type conductivity. The $|S|$ value decreased almost proportionally from 150 to 20 $\mu \text{V K}^{-1}$ with $\log n_{3D}$. We calculated the $|S|$ - $\log n_{3D}$ relationship for anatase TiO₂ based on the assumption that the DOS around the conduction band bottom is

parabolic with a density of state effective mass of $1.25 m_0$ where m_0 is the free electron mass, for comparison.²⁴ Although the slope of the calculated $|S|$ - $\log n_{3D}$ line ($n_{3D} < 10^{20} \text{ cm}^{-3}$) corresponded to $-\ln 10 \cdot k_B/e$ ($= -198 \mu\text{VK}^{-1}$), that of the observed line was an order magnitude smaller ($-20 \mu\text{VK}^{-1}$). In the higher n_{3D} region ($n_{3D} > 10^{20} \text{ cm}^{-3}$), the observed $|S|$ values corresponded well to the calculated line. These results clearly indicate that the DOS around the conduction band bottom of the TiO_2 epitaxial film is not parabolic.

To further clarify the DOS shape around the conduction band bottom, we subsequently fabricated a top-gate TFT using a TiO_2 anatase epitaxial film (undoped, 30 nm thick). First, metallic Ti films (20 nm thick) were deposited for use as the source and drain electrodes. Deposition was performed through a stencil mask by electron beam (EB) evaporation (base pressure $\sim 10^{-4}$ Pa, no substrate heating). Second, a 200 nm thick Y_2O_3 film (polycrystalline, dielectric permittivity $\epsilon_r=20$) was deposited through a stencil mask by PLD ($\sim 3 \text{ J cm}^{-2} \text{ pulse}^{-1}$, oxygen pressure ~ 1 Pa) using a dense polycrystalline Y_2O_3 ceramic as the target. Finally, a gate electrode, which was a metallic Ti film (20 nm thick), was deposited through a stencil mask by EB evaporation. The resultant TFT was annealed at 200°C in air to reduce the oxygen defects generated during the Y_2O_3 deposition.

The transistor characteristics of the resultant TiO_2 TFT were measured with a semiconductor device analyzer (B1500A, Agilent Technologies) at RT. The channel length (L) and channel width (W) of the TFT were both $400 \mu\text{m}$. Figures 3(a) and (b) show typical transistor characteristics of a TiO_2 -TFT [(a) drain current (I_d)-drain voltage (V_d) and (b) I_d - V_g curves]. Figure 3(a) clearly shows the current saturation and pinch off behavior, indicating that TFTs obey standard field effect theory. I_d of the TFT increased as V_g increased; hence, the channel was n -type and electron carriers were accumulated by positive V_g [Fig. 3(b)]. The on-off current ratio was $>10^4$. The

calculated threshold voltage was -17 V from the $I_d^{0.5}-V_g$ plot [inset of (b)]. The μ_{FE} values were obtained from $\mu_{FE}=g_m[(W/L)C_iV_d]^{-1}$ where g_m is transconductance $\partial I_d/\partial V_g$ and C_i is the capacitance per unit area (89 nFcm $^{-2}$). The μ_{FE} values of this TFT increased with V_g , and reached ~ 0.9 cm 2 V $^{-1}$ s $^{-1}$ (Fig. 4).

We then measured the field-modulated S of the TiO $_2$ TFT using two Peltier devices to introduce a temperature difference (ΔT up to 3 K) between the source and drain electrodes. Details of the thermopower measurement are described elsewhere.^{14, 15} Figure 4 shows the $|S|-V_g$ plots for the TiO $_2$ TFT. The negative S values confirmed the channel is an n -type. The $|S|$ value gradually increased from 330 to 390 μ VK $^{-1}$ as V_g increased in the lower V_g region ($V_g < 12$ V), and the sheet carrier concentration increased. On the other hand, in the higher V_g region ($V_g > 12$ V), the $|S|$ value gradually decreased with V_g . As discussed above, the $|S|$ values should decrease with V_g because the carrier concentration increases with V_g for a parabolic DOS shape around the conduction band bottom. Because a small transition of I_d was also observed at $V_g \sim 12$ V in the I_d-V_g curve [Fig. 3(b)], the electronic states of the channel returned to the original DOS parabolic shape upon applying $V_g > 12$ V.

These results indicate the DOS around the conduction band bottom for a TiO $_2$ epitaxial film is composed of not only the original parabolic DOS (high μ), but also small non-parabolic shaped DOS such as a tail state (low μ) hybridized near the conduction band bottom.

In summary, we have shown that the thermopower (S) measurements for anatase TiO $_2$ epitaxial films (undoped and Nb-doped, carrier concentration, n_{3D} : $10^{17}-10^{21}$ cm $^{-3}$) are effective to experimentally clarify the electronic density of states (DOS) near the conduction band bottom. The slope of the $|S|-\log n_{3D}$ plots for anatase TiO $_2$ films is -20 μ VK $^{-1}$, which is an order magnitude smaller than that of semiconductors with parabolic DOS (-198 μ VK $^{-1} = \ln 10 \cdot k_B/e$), and the $|S|$ values for TFTs increase with V_g in the

low V_g region. The DOS around the conduction band bottom for an TiO_2 epitaxial film is composed of both the parabolic shaped original DOS (high μ) and a small non-parabolic shaped DOS such as a tail state (low μ) hybridized near the conduction band bottom.

Some of this work was financially supported by MEXT (22360271, 22015009).

References

- ¹A. Fujisjima and K. Honda, *Nature* **238**, 37 (1972).
- ²B. O'Regan and M. Grätzel, *Nature* **353**, 737 (1991).
- ³X. Chen and S. S. Mao, *Chem. Rev.* **107**, 2891 (2007).
- ⁴R. Sanjines, H. Tang, H. Berger, F. Gozzo, G. Margaritondo and F. Levy, *J. Appl. Phys.* **75**, 2945 (1994).
- ⁵A. G. Thomas, W. R. Flavell, A. R. Kumarasinghe, A. K. Mallick, D. Tsoutsou, G. C. Smith, R. Stockbauer, S. Patel, M. Grätzel and R. Hengerer, *Phys. Rev. B* **67**, 035110 (2003).
- ⁶A. G. Thomas, W. R. Flavell, A. K. Mallick, A. R. Kumarasinghe, D. Tsoutsou, N. Khan, C. Chatwin, S. Rayner, G. C. Smith, R. L. Stockbauer, S. Warren, T. K. Johal, S. Patel, D. Holland, A. Taleb and F. Wiame, *Phys. Rev. B* **75**, 035105 (2007).
- ⁷A. Sandell, B. Sanyal, L. E. Walle, J. H. Richter, S. Plogmaker, P. G. Karlsson, A. Borg and P. Uvdal, *Phys. Rev. B* **78**, 075113 (2008).
- ⁸A. E. Taverner, P. C. Hollamby, P. S. Aldridge, R. G. Egdell and W. C. Mackrodt, *Surface Science* **287**, 653 (1993).
- ⁹Shang-Di Mo and W. Y. Ching, *Phys. Rev. B* **51**, 13023 (1995).
- ¹⁰R. Asahi, Y. Taga, W. Mannstadt and A. J. Freeman, *Phys. Rev. B* **61**, 7459 (2000).
- ¹¹L. Chiodo et al., *Phys. Rev. B* **82**, 045207 (2010).
- ¹²P. D. Johnson and S. L. Hulbert, *Rev. Sci. instrum.* **61**, 2277 (1990).

- ¹³K. P. Pernstich, B. Rössner and B. Batlogg, *Nature Mater.* **7**, 321 (2008).
- ¹⁴H. Ohta, Y. Masuoka, R. Asahi, T. Kato, Y. Ikuhara, K. Nomura, and H. Hosono, *Appl. Phys. Lett.* **95**, 113505 (2009).
- ¹⁵A. Yoshikawa, K. Uchida, K. Koumoto, T. Kato, Y. Ikuhara, and H. Ohta, *Appl. Phys. Express* **2**, 121103 (2009).
- ¹⁶J. C. Hulteen and C. R. Martin, *J. Mater. Chem.* **7**, 1075 (1997).
- ¹⁷Y. Matsumoto, M. Murakami, T. Shono, T. Hasegawa, T. Fukumura, M. Kawasaki, P. Ahmet, T. Chikyow, S. Koshihara and H. Koinuma, *Science* **291**, 854 (2001).
- ¹⁸Y. Furubayashi, T. Hitosugi, Y. Yamamoto, K. Inaba, G. Kinoda, Y. Hirose, T. Shimada and T. Hasegawa, *Appl. Phys. Lett.* **86**, 252101 (2005).
- ¹⁹M. Katayama, S. Ikesaka, J. Kuwano, H. Koinuma and Y. Matsumoto, *Appl. Phys. Lett.* **92**, 132107 (2008).
- ²⁰M. Katayama, H. Koinuma and Y. Matsumoto, *Mater. Sci. Eng. B* **148**, 19 (2008).
- ²¹L. Forro, O. Chauvet, D. Emin, L. Zuppiroli, H. Berger and F. Levy, *J. Appl. Phys.* **75** 633 (1994).
- ²²D. Kurita, S. Ohta, K. Sugiura, H. Ohta and K. Koumoto, *J. Appl. Phys.* **100**, 096105 (2006).
- ²³H. Ohta, S-W. Kim, Y. Mune, T. Mizoguchi, K. Nomura, S. Ohta, T. Nomura, Y. Nakanishi, Y. Ikuhara, M. Hirano, H. Hosono and K. Koumoto, *Nature Mater.* **6**, 129 (2007).
- ²⁴H. Ohta, K. Sugiura and K. Koumoto, *Inorg. Chem.* **47**, 8429 (2008).

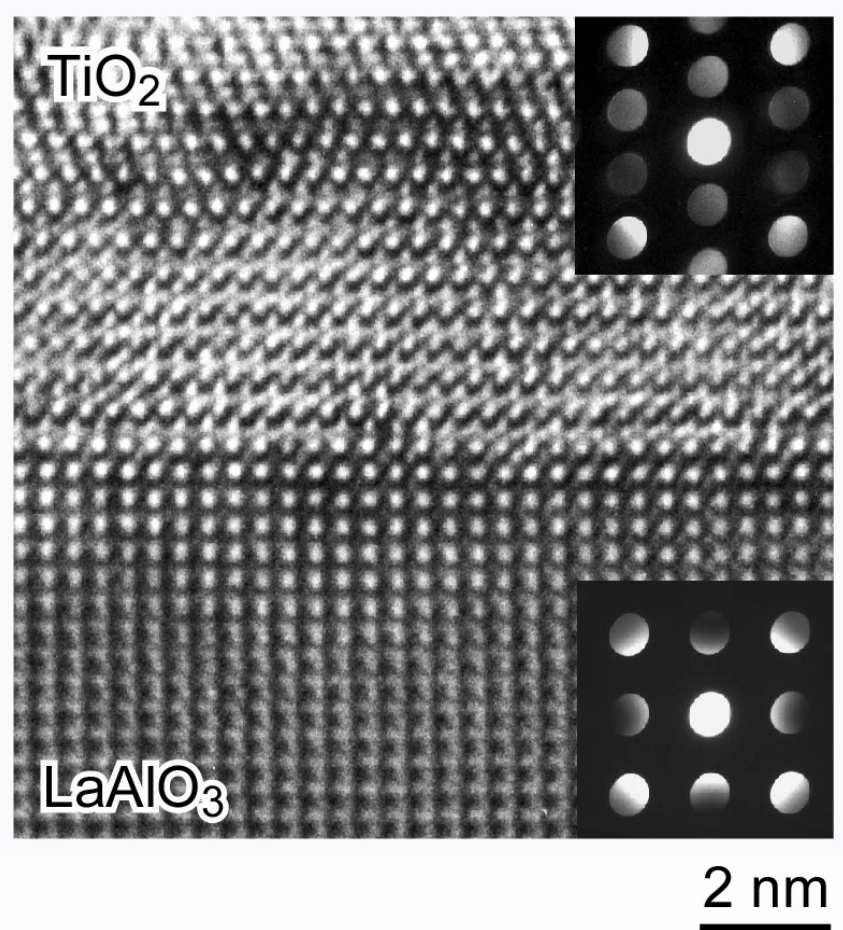


Fig. 1 Cross sectional HRTEM image of the TiO_2 epitaxial film grown on a (001) LaAlO_3 substrate with an epitaxial relationship $(001)[100]\text{TiO}_2 \parallel (001)[100]\text{LaAlO}_3$. Nanobeam electron diffraction patterns for the TiO_2 and LaAlO_3 are also shown.

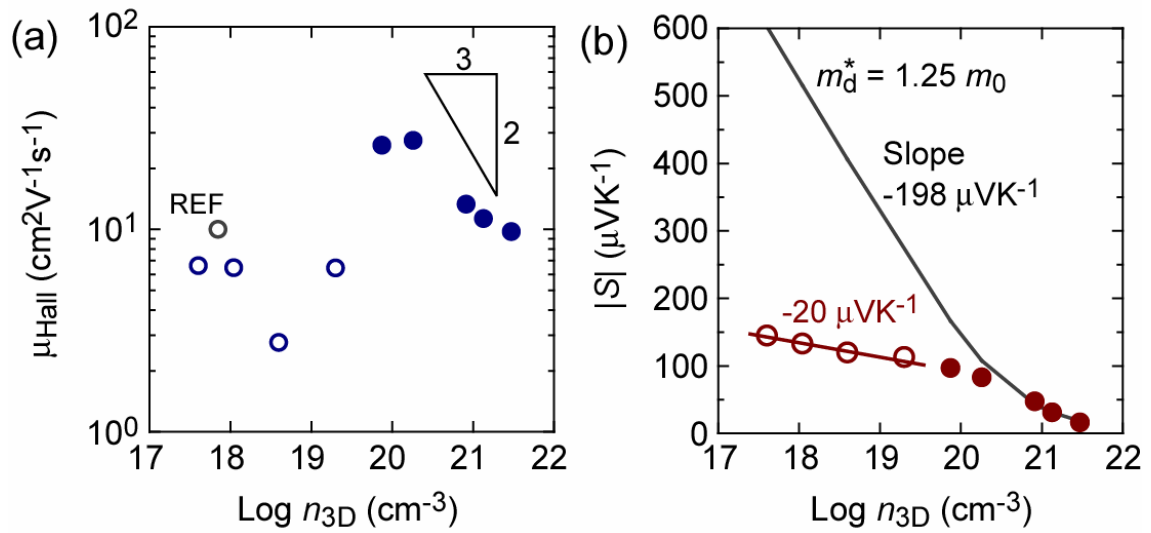


Fig. 2 Carrier concentration ($n_{3\text{D}}$) dependence of (a) Hall mobility (μ_{Hall}) and (b) thermopower ($|S|$) for TiO₂ epitaxial films (undoped and Nb-doped, ~ 100 nm thick) grown on (001) LaAlO₃. For comparison, μ_{Hall} of a bulk single crystal (REF 21) is plotted in (a) and the calculated $|S|$ - $\log n_{3\text{D}}$ relationship for anatase TiO₂ is shown in (b).

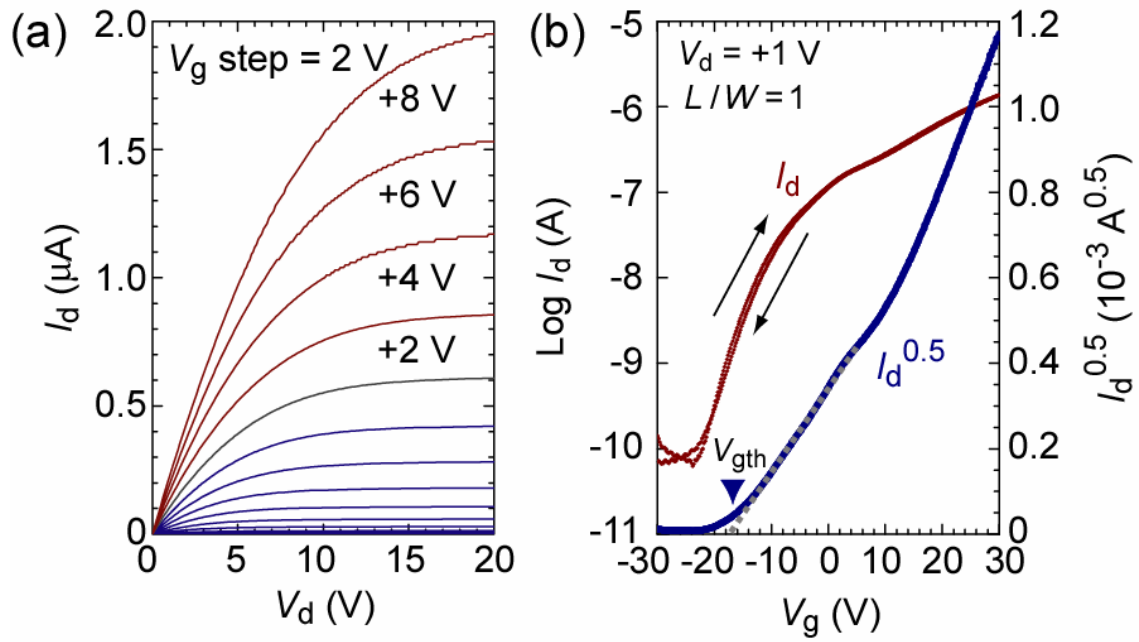


Fig. 3 Typical transistor characteristics [(a) I_d - V_d and (b) I_d - V_g curves] of a TiO₂ TFT at RT. Current saturation and pinch off behavior are clear in (a). $I_d^{0.5}$ - V_g plots are shown in (b). On-off current ratio is $>10^4$ and V_{gth} is -17 V.

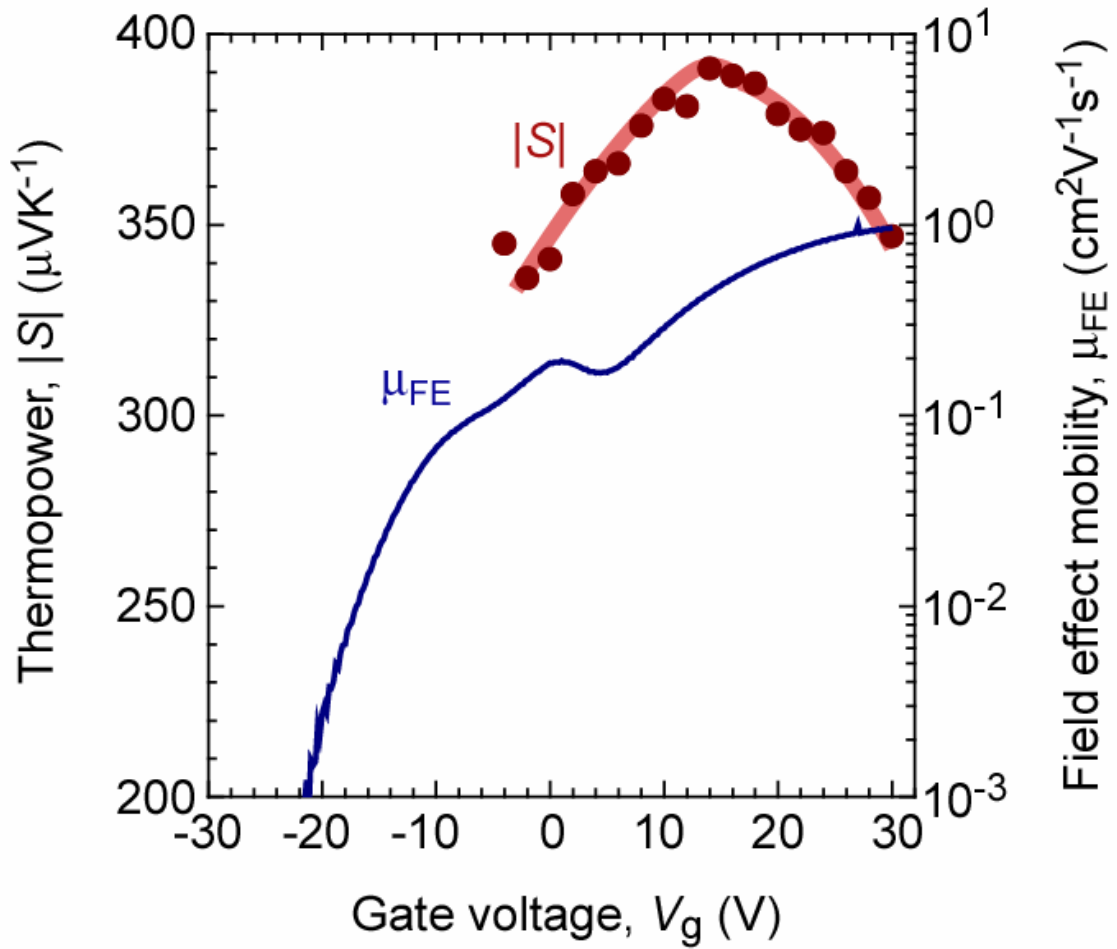


Fig. 4 Field modulation of thermopower, $|S|$ - V_g plots of TiO_2 TFTs at RT. μ_{FE} - V_g plots are also shown. As V_g increases in the lower V_g region ($V_g < 12$ V), the $|S|$ value gradually increases from 330 to 390 μVK^{-1} , whereas the $|S|$ value gradually decreases with V_g in the higher V_g region ($V_g > +12$ V). As V_g increases, μ_{FE} gradually increases.